EEET ECOLOGICAL ENGINEERING & ENVIRONMENTAL TECHNOLOGY

Ecological Engineering & Environmental Technology, 2026, 27(4), 79–95
https://doi.org/10.12912/27197050/21842
ISSN 2719–7050, License CC-BY 4.0

Received: 2026.02.13
Accepted: 2026.03.16
Published: 2026.04.01

Simulating hydrological response and flow regime dynamics to land cover changes in sub-watershed

Ahmad Tahir[1*], Andang Suryana Soma[2], Usman Arsyad[2]

[1] Faculty of Forestry, Hasanuddin University, Makassar, Indonesia
[2] Department of Forestry, Faculty of Forestry, Hasanuddin University, Makassar, South Sulawesi 90245, Indonesia
* Corresponding author's e-mail: tahyr102@gmail.com

ABSTRACT

Land degradation in tropical forest regions due to anthropogenic activities and land cover change poses a serious challenge to the hydrological stability of watersheds. This study aims to (1) analyze the dynamics of land cover change in the Manggululiling sub-watershed, South Sulawesi, during the 2020–2024 period, and (2) evaluate the hydrological stability of the area based on the river regime coefficient (RRC) values through the soil and water assessment tool (SWAT) model simulation. The methods used include Landsat 8 OLI image interpretation for land cover analysis and hydrological modeling using SWAT by dividing the watershed into hydrologic response units (HRUs). Land classification validation was conducted using the confusion matrix method, which resulted in an overall accuracy rate above 97%. Watershed health indicators were assessed based on the river regime coefficient and runoff coefficient in accordance with Ministry of Forestry regulations. The results show that the Manggululiling sub-watershed has a high level of ecological resilience against deforestation pressure. Primary Dryland Forest remained stable at 915.65 ha (47.97%) throughout the observation period. Positive vegetation dynamics occurred in the form of an increase in Secondary Dryland Forest by 5.11 ha through natural succession processes from open land. Other land-use changes included the conversion of paddy fields into mixed dryland agriculture covering 23.24 ha. Hydrologically, the area is in a stable condition as reflected by the constant average curve number (CN) value (~60.13) and the dominance of lateral flow over surface runoff. Despite extreme rainfall anomalies in 2024 that increased maximum discharge, baseflow availability remained well-maintained. In conclusion, the preservation of primary forest cover in the upstream area is crucial for maintaining water regulation functions and mitigating the risk of hydrometeorological disasters in the Manggululiling sub-watershed.

Keyword: SWAT, land cover change, river regime coefficient, Manggululiling sub-watershed, hydrological stability.

INTRODUCTION

Land degradation is a global phenomenon driven by various anthropogenic activities and natural processes, including deforestation, land cover change, and soil erosion. These processes significantly disrupt the hydrological cycle by altering infiltration and evapotranspiration rates, which ultimately limits water availability and increases the risk of hydrometeorological disasters (Pindi and Jayakumar, 2023). In tropical forest regions, land cover change particularly the conversion of forests into agricultural areas or settlements has rapid and widespread impacts on the hydrological response of watersheds, affecting both surface runoff and base flow (Latue et al., 2023). Therefore, understanding the dynamics of land cover change is crucial for efforts to mitigate environmental damage.

The Segeri watershed in Indonesia constitutes a priority area designated for rehabilitation by regional authorities. With a total area of approximately 16,645.29 ha, this watershed is characterized by declining land function, degraded water quality, and weak water management infrastructure. Specifically, the Manggululiling sub-watershed

(1,908.88 ha), which forms part of the Segeri system, faces complex environmental pressures. In addition to land conversion driven by community occupation, this area serves as a location for active river stone mining. This extractive activity has the potential to damage river morphology, trigger bank erosion, and increase sedimentation (Karouw et al., 2016; Sayed et al., 2025). These human interventions threaten the sustainability of hydrological functions and the well-being of stakeholders who rely on these water resources (Miralles-Wilhelm et al., 2023).

Given the complex interactions between land cover change, mining activities, and hydrological responses in the Manggululiling Sub-watershed, direct field measurement is often limited by spatial and temporal constraints. Consequently, a hydrological modeling approach is required. The soil and water assessment tool (SWAT) is a physically-based model proven to be reliable in analyzing watershed responses to long-term environmental changes across various soil conditions, slopes, and land management practices (Soma et al., 2021). SWAT operates by dividing the watershed into hydrologic response units (HRUs) to precisely estimate water balance components (Nursaputra et al., 2024). The selection of SWAT for the Manggululiling sub-watershed is based on its capability to comprehensively represent the specific impacts of land degradation on runoff and sediment yield.

To quantify the degree of hydrological stability resulting from these changes, a measurable indicator is necessary. The river regime coefficient (RRC), locally known as Koefisien Regim Aliran (KRA), is utilized as the primary indicator for assessing the hydrological quality of a watershed. The RRC value is calculated based on the ratio between the maximum discharge $Q_{\{max\}}$ and the minimum discharge $Q_{\{min\}}$ of the river, which is heavily influenced by physical characteristics such as soil type and vegetation cover (Hidayat et al., 2025; Hidayat, 2023). A higher RRC value indicates a wider gap between flood and drought discharges, signifying low hydrological stability and a reduced capacity of the watershed to store water.

Although various studies have discussed the general degradation of the Segeri watershed, specific evaluations regarding the combined impact of land cover change and extractive activities on hydrological stability in the Manggululiling sub-watershed using the RRC approach remain limited. The objectives of this study are: (1) to analyze the dynamics of land cover change in the Manggululiling sub-watershed, and (2) to evaluate the hydrological stability of the region based on RRC values derived from SWAT model simulations. The results of this research are expected to provide a scientific basis for formulating precise land management and rehabilitation strategies, particularly within the context of ecological engineering in degraded tropical watersheds.

METHOD

Study area

This study focuses on the Manggululiling sub-watershed, an integral part of the Segeri watershed system covering a total area of 1,908.88 ha, which administratively encompasses the jurisdictions of Barru Regency and Pangkajene and Islands Regency as spatially illustrated in Figure 1. Ecologically, the area represents a typical tropical rainforest typology characterized by high annual rainfall intensity and significant humidity, supporting the growth of dense, broad-leaved evergreen vegetation with a complex stratified canopy structure. This vegetation plays a crucial role in regulating the hydrological cycle through rainfall interception and soil infiltration processes, although its functional integrity currently faces dynamic pressures from surrounding anthropogenic activities.

Data Preparation

Spatial data preparation and DEM processing

The digital elevation model (DEM) was constructed using the Topo to Raster interpolation method to ensure hydrological continuity, which is crucial for the accuracy of the SWAT simulation. The interpolation inputs integrated the Manggululiling sub-watershed boundary, river network vector layers, and 20-m interval contours extracted from the high-resolution (8-m) national digital elevation model (DEMNAS). To maintain consistency with other spatial datasets, the resulting DEM was projected onto the Universal Transverse Mercator (UTM) coordinate system and resampled to a 30-m spatial resolution.

Land cover analysis

Land cover datasets were derived through the interpretation of Landsat 8 OLI imagery spanning

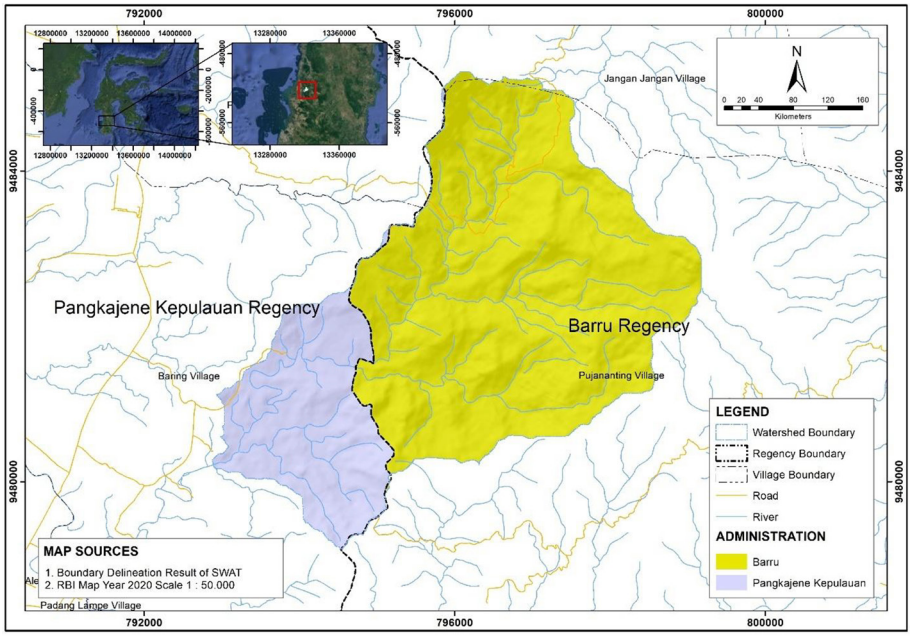

Figure 1. Administrative map of the Manggululiling sub-watershed

the 2020 and 2024 periods. The classification process was focused on the previously delineated sub-watershed boundaries. To ensure data reliability, land classification validation was conducted using the Confusion Matrix method against ground-truth points and Google Earth historical imagery, achieving an overall accuracy rate above 95%.

Soil data

Soil data were obtained from the RePPProT (Regional Physical Planning Programme for Transmigration) database. These data were parameterized within the SWAT framework, with a specific focus on the following variables: soil texture, erodibility (K-factor), and organic matter content. All soil attributes were compiled into the SWAT soil database format to accurately simulate infiltration and runoff processes within each hydrologic response unit (HRU).

Climate data

The SWAT model was driven by daily meteorological records for the 2015–2024 period. Climate variables, including precipitation, maximum and minimum temperature, relative humidity, solar radiation, and wind speed, were sourced from the NASA POWER dataset. These data were extracted and integrated based on the specific coordinates of the Manggululiling sub-watershed to ensure representative climatic input for the hydrological simulation.

SWAT model setup and integration

All spatial datasets were harmonized within the ArcGIS 10.8.2 environment prior to their integration into the SWAT model. The model used in this study is the SWAT 2012 version. The sub-watershed delineation was performed and further subdivided into hydrologic response units (HRUs) based on the unique combination of land cover, soil type, and slope. The overall sequence of data processing, land cover analysis, and hydrological simulation employed in this study is illustrated in Figure 2.

Analysis of land cover change

Image processing and classification

Land cover dynamics were analyzed using Landsat 8 OLI/TIRS datasets (30 m resolution) acquired in 2020 and 2024. The image processing workflow comprised pre-processing (gap filling, cropping) and the generation of a false color composite (FCC) using bands 6, 5, and 4 to optimize vegetation discrimination. Land cover classes were categorized according to the Indonesian National Standard (SNI No. 1/PSDH/PLA.1/7/2020). A post-classification comparison was conducted using spatial overlay analysis to quantify the transition of land cover types and calculate the areal extent of changes over the study period.

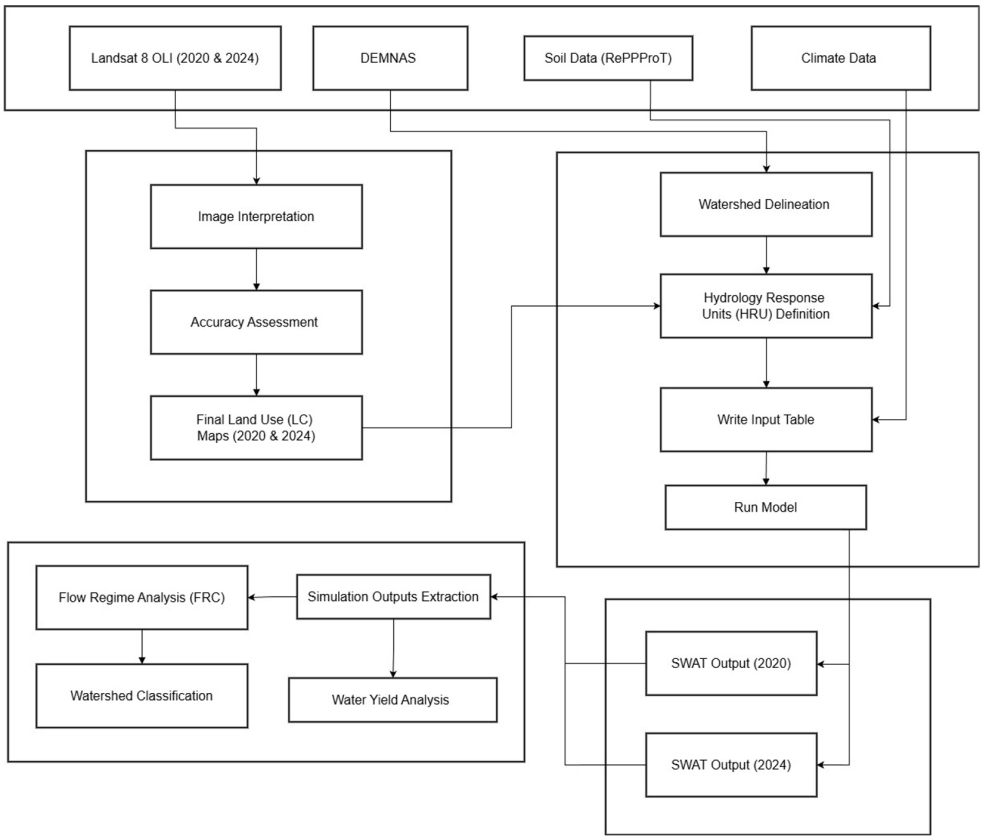

Figure 2. Workflow analitycal steps

Accuracy assessment

To validate the classification results, an accuracy assessment was performed by cross-referencing the classified maps with ground truth data. Due to the retrospective nature of the 2020 dataset, which precluded direct field verification, validation was conducted using high-resolution historical imagery from Google Earth Pro as a proxy for ground truth (Tilahun, 2015). The minimum sample size (N) for accuracy assessment was determined using the Estok Navitte Cowan formula (Equation 1):

$$n = \frac{z^2[p(1-p)]N}{z^2[p(1-p)] + (N-1)E^2} \qquad (1)$$

In this equation, n denotes the calculated sample size. The variable Z represents the reliability coefficient (standard normal deviate), set at 1.65 to correspond with a 90% confidence level. The term $p(1-p)$ expresses the population variability as a proportion, while E signifies the allowable margin of error. Finally, N refers to the population size, defined in this study as the total area of each specific land cover class. The accuracy of image interpretation was evaluated using the confusion matrix method, as presented in Table 1. The acceptable accuracy level for image interpretation is greater than 85%.

The columns (A, B, C) represent the reference data derived from ground truth observations, while the rows (A', B', C') correspond to the classified data generated from the image interpretation. The diagonal elements, denoted as Xnn and Xkk, indicate the number of correctly classified samples where the map class agrees with the reference class. The row total (Xk+) signifies the total number of pixels classified into a specific category (used to calculate commission error), whereas the column total (X+k) represents the actual total of reference samples for that category (used to calculate omission error). The value N denotes the total sample size used in the accuracy assessment.

SWAT model configuration and simulation

Watershed delineation and HRU definition

The watershed delineation was executed using the automatic delineator in ArcSWAT. A threshold drainage area of 85 ha was applied to define the stream network, resulting in the discretization of the watershed into 9 sub-basins. Subsequently,

Table 1. Confussion matrix

Parameter	Reference data				Row total
		A	B	C	
Classified data	A`	X_{nn}			X_{K+}
	B`				
	C`			X_{KK}	
Colomn total		X_{+K}			N

HRUs were generated by overlaying land use, soil, and slope datasets. To capture the spatial heterogeneity of the watershed, a multiple HRU approach was adopted with threshold percentages of 0% for land use, soil, and slope classes, respectively. This detailed configuration resulted in a total of 501 HRUs (2020) 515 HRUs (2024).

Simulation setup and scenarios

The simulation was conducted for the period of 2020 to 2024. No warm-up period was applied (NYSKIP = 0), and the entire simulation duration was utilized for analysis. Two distinct scenarios were executed to evaluate the impact of land cover dynamics: (1) Baseline scenario using the 2020 land cover map; and (2) Impact scenario using the 20200 and 2024 land cover map. Meteorological inputs were kept constant across both scenarios to isolate the hydrological response attributed solely to land cover changes.

Water yield calculation

The primary output analyzed is water yield (*WYLD*), representing the net amount of water leaving the HRU and contributing to the main reach. The calculation follows the water balance equation 2 (Arnold et al., 2011):

$$WYLD = SURQ + LATQ + \\ + GWQ - TLOSS - pond\ abstractions \quad (2)$$

where: *WYLD* (mm) is the net amount of water leaving the HRU and contributing to the main reach. It is calculated as the sum of surface runoff (*SURQ*), lateral flow (*LATQ*), and base flow (*GWQ*), less any transmission losses (*TLOSS*) and pond abstractions.

Water discharge and flow regime analysis

To evaluate the hydrological stability of the watershed under different land cover conditions, the *FRC* was analyzed based on the SWAT simulation outputs. The *FRC* serves as a key indicator of watershed health, reflecting the disparity between peak and base flows. The coefficient is calculated as the ratio of maximum to minimum discharge, following the formula mandated by the Indonesian Ministry of Forestry Regulation No. P.61/Menhut-II/2014:

$$FRC = \frac{Q_{\{max\}}}{Q_{\{min\}}} \quad (3)$$

where: *FRC* is the river regime coefficient (dimensionless), $Q_{\{max\}}$ is the maximum annual discharge (m^3/s), and $Q_{\{min\}}$ is the minimum annual discharge (m^3/s).

The *FRC* varies significantly when calculated using these annual maximum and minimum discharge values (Hidayat, 2023). Despite this variability, this study adopts the calculation method and classification standards mandated by the Indonesian Ministry of Forestry Regulation No. P.61/Menhut-II/2014. A lower *FRC* value indicates better hydrological conditions, characterized by a stable flow with sufficient baseflow during dry periods and controlled runoff during wet periods. The classification of watershed health based on *FRC* values is presented in Table 2.

Surface runoff coefficient analysis

To identify the factors driving discharge fluctuations, a further analysis was conducted using the runoff coefficient (*C*). This value represents the percentage of precipitation that converts into surface runoff due to the soil's limited infiltration capacity. The value of *C* was calculated using the water balance method based on the annual SWAT simulation results, defined as the ratio of total annual surface runoff depth to total annual precipitation depth (Asdak, 2010):

$$C = \frac{R}{P} \quad (4)$$

Table 2. Classification of river regime coefficient (RRC)

Value	Classes
RRC < 10	Very low
10 < RRC ≤ 50	Low
50 < RRC ≤ 80	Medium
80 < RRC ≤ 110	High

Note: Regulation of the Minister of Forestry No: P.61/Menhut-II/2014.

Table 3. Classification of surface runoff coefficient (*C*)

Value	Classification	Health category
C < 0.20	Very low	Good (healthy)
0.20 < C ≤ 0.40	Medium	Moderate
>0.40	High	Poor (degraded)

Note: Regulation of the Minister of Forestry No. P.61/Menhut-II/2014.

In the equation above, *C* denotes the dimensionless runoff coefficient, *R* represents the total depth of surface runoff generated annually (mm), and *P* represents the total depth of annual precipitation (mm).

The calculated *C* values were subsequently classified to assess the hydrological health of the watershed. This assessment was conducted in accordance with the standard criteria outlined in the Regulation of the Minister of Forestry of the Republic of Indonesia Number P.61/Menhut-II/2014 regarding Monitoring and Evaluation of Watershed Management. The classification standards are presented in Table 3.

RESULT AND DISCUSSION

Biophysical characteristics

The Manggululiling sub-watershed encompasses a total area of 1,908.88 ha, administratively spanning the regencies of Barru and Pangkajene dan Kepulauan. Topographically, the Manggululiling Sub-watershed is characterized by rugged terrain with a distinct dominance of steep slopes. The spatial analysis reveals that the 25–45% slope class covers the largest portion of the area, spanning 1,294.70 ha and accounting for 67.82% of the total watershed. When combined with the very steep class (>45%), which occupies 180.92 ha (9.48%), it is evident that over 77% of the basin exhibits a slope gradient greater than 25%. In comparison, gentler slopes (8–15% and 15–25%) make up only a small part of the area, at 8.75% and 13.96%. This steep terrain means water flows down quickly, naturally increasing the risk of high surface runoff and erosion. Recent studies confirm that steeper slopes significantly increase cumulative runoff, with erosion rates intensifying rapidly beyond a critical slope of 10° (Zheng et al., 2019). The spatial distribution of these slope classes is presented in Figure 3.

Soil physical properties play a vital role in determining the hydrological response and erosion vulnerability of a watershed. Based on spatial analysis presented in Figure 4, the soil composition in the Manggululiling sub-watershed is clearly dominated by two major mapping units: Soil 10 and Soil 3 (Table 4). Soil 10 covers the largest area (31.63%), followed closely by Soil 3 (30.91%). Cumulatively, these two units encompass over 62% of the total watershed area. Physically, both dominant units share similar characteristics; they are classified as Dystropepts with primary textures of Silty Clay (SiC) and Silt Loam (SiL).

These soil texture conditions have direct implications for water and sediment movement. Rainfall impact on these soil types causes soil particles to detach easily from their aggregates, which are subsequently transported by surface flow to lower elevation (Sari and Jamilah, 2023). This issue is further exacerbated by the high clay content within the soil texture. As demonstrated by (Bashari et al., 2013), soils with significant clay content exhibit low infiltration rates, which consequently increases the volume of surface runoff. Therefore, the dominance of soils that are both easily detachable and impermeable renders the study area highly susceptible to flow regime instability, characterized by rapid runoff generation and high erosion risk.

In general, the study area is characterized by a wet climate with abundant annual water availability. Based on the analysis of ten years of historical data (2015–2024) extracted from the NASA POWER database, the average areal rainfall in this watershed is recorded at 2,066.86 mm/year. This value was derived by averaging data from four virtual station points distributed spatially to represent rainfall variability from upstream to downstream.

The monthly rainfall distribution follows a distinct Monsoonal pattern, marked by a sharp contrast between the wet and dry seasons

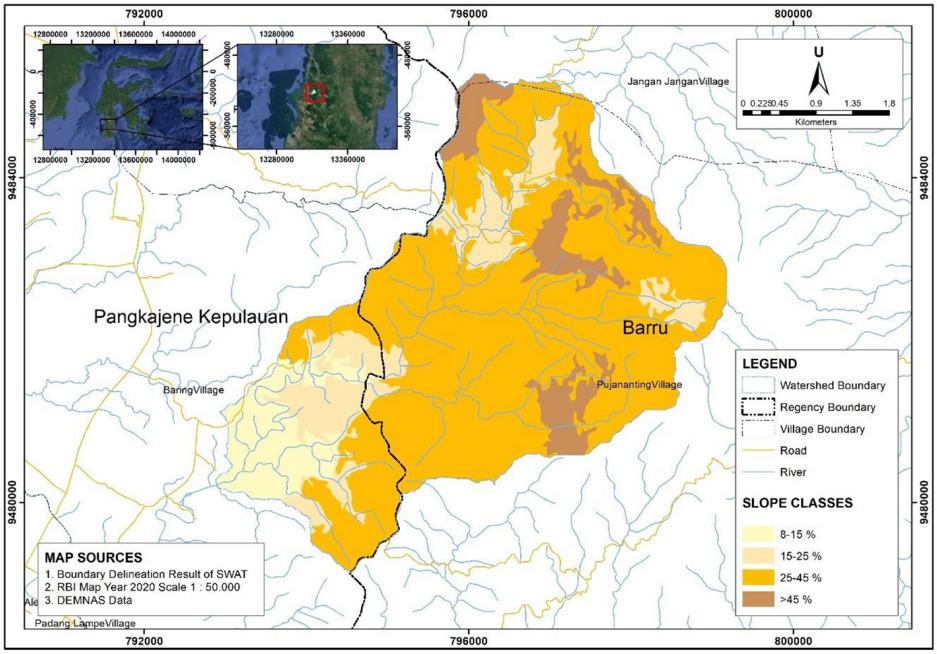

Figure 3. Slope map of the slope of the Manggululiling sub-watershed

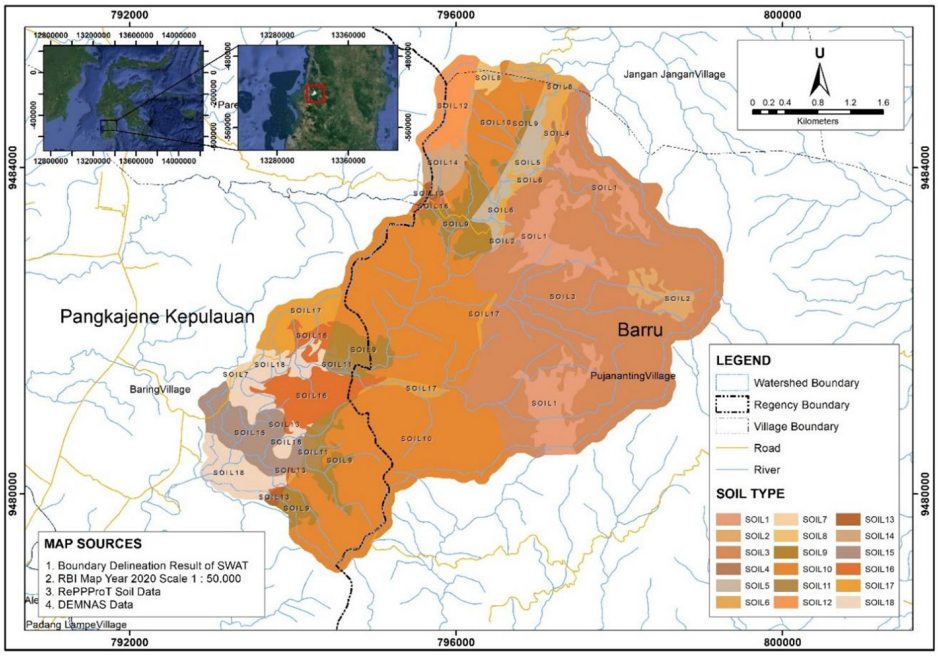

Figure 4. Soil map of Manggululiling sub-watershed

(Susanto, 2003). As presented in Figure 5, the wet phase occurs at the turn of the year, with peak precipitation in December (377.18 mm/month) and January (355.61 mm/month). This high rainfall intensity serves as a primary hydrological trigger; when abundant rainwater interacts with saturated clay soils, it significantly increases the potential for surface runoff generation. Entering the mid-year period, the hydrological condition shifts drastically into a water deficit phase. Rainfall intensity declines sharply, reaching its lowest levels in August (36.40 mm/month) and September (42.06 mm/month). This stark contrast between the wet and dry seasons presents a dual challenge for the watershed: beyond the threat of flooding, there is a significant risk of meteorological drought that could compromise river baseflow stability.

Table 4. Soil types in Mangguliling Sub-watershed

Soil unit	Soil group	Area (Ha)	Slope (%)	Percentage (%)
SOIL 1	Dystropepts; Eutropepts	138.28	>45%	7.24
SOIL 2	Dystropepts; Eutropepts	28.23	15–25%	1.48
SOIL 3	Dystropepts; Eutropepts	590.02	25–45%	30.91
SOIL 4	Dystropepts; Eutropepts; Tropudalfs;	1.51	>45%	0.08
SOIL 5	Dystropepts; Eutropepts; Tropudalfs;	41.27	15–25%	2.16
SOIL 6	Dystropepts; Eutropepts; Tropudalfs;	33.97	25–45%	1.78
SOIL 7	Dystropepts; Eutropepts; Tropudalfs;	0.51	8–15%	0.03
SOIL 8	Dystropepts; Tropudults; Humitropepts	6.38	>45%	0.33
SOIL 9	Dystropepts; Tropudults; Humitropepts	117.53	15–25%	6.16
SOIL 10	Dystropepts; Tropudults; Humitropepts	603.82	25–45%	31.63
SOIL 11	Dystropepts; Tropudults; Humitropepts	21.71	8–15%	1.14
SOIL 12	Dystropepts; Tropudults; Troperthents	34.50	>45%	1.81
SOIL 13	Dystropepts; Tropudults; Troperthents	5.02	15–25%	0.26
SOIL 14	Dystropepts; Tropudults; Troperthents	23.92	25–45%	1.25
SOIL 15	Dystropepts; Tropudults; Troperthents	60.66	8–15%	3.18
SOIL 16	Tropudults; Dystropepts; Haplorthox	74.42	15–25%	3.90
SOIL 17	Tropudults; Dystropepts; Haplorthox	43.07	25–45%	2.26
SOIL 18	Tropudults; Dystropepts; Haplorthox	84.05	8–15%	4.40

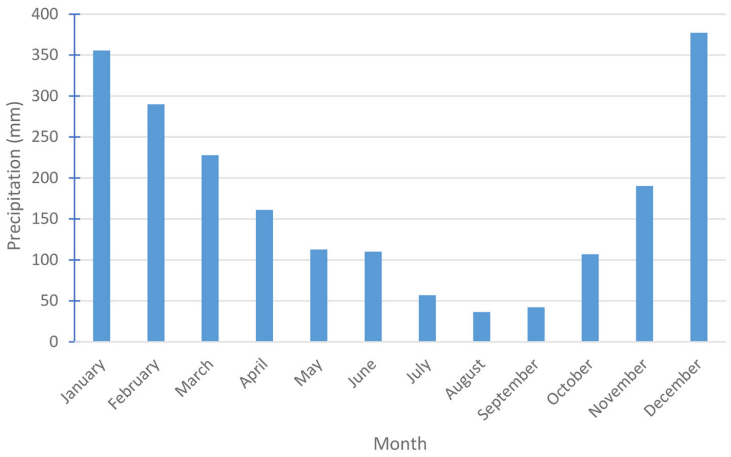

Figure 5. Average monthly rainfall distribution in the Mangguliling Sub-watershed (2015–2024)

Land cover change analysis

Accuracy assessment

Validation of classification results is a crucial stage to ensure the reliability of land cover maps before they are utilized for change analysis and hydrological modeling. Given the historical nature of the 2020 dataset, direct field verification was not feasible; therefore, validation was conducted through visual interpretation of high-resolution historical imagery from Google Earth Pro as a proxy for ground truth (Tilahun, 2015). For the 2024 dataset, this approach was complemented by 2025 field observations to ensure temporal consistency.

Accuracy assessment utilized the Confusion Matrix method to measure the agreement between classification results and reference data. The minimum sample size was determined based on the Estok Navitte Cowan equation with a 90% confidence level, resulting in 184 sample points for both 2020 and 2024. These points were distributed using the stratified random sampling method across all land cover classes to ensure adequate representation of the entire study area.

Based on the confusion matrix calculations in Table 5 and Table 6, the classification demonstrates an overall accuracy of 97.83% for the 2020 land cover map, while the 2024 map achieved an accuracy of 98.37%. Both values significantly exceed the standard acceptable threshold of 85%.

Most land cover classes, such as values reaching 100%. Minor classification discrepancies primary dryland forest, settlements, and savanna, demonstrate very high accuracy with user's accuracy were found in the Shrub and Paddy Field categories. In 2024, the Shrub class had a Producer's Accuracy of 71.43%, where some points were misclassified into the paddy field and secondary dryland forest classes. Such discrepancies are common in remote sensing due to the similarity in spectral reflectance between low-density vegetation and certain plant growth phases. Nevertheless, with overall accuracy values reaching 97.83% (2020) and 98.37% (2024), the resulting land cover maps are declared valid and statistically reliable for use as spatial inputs in subsequent land cover change analysis and SWAT simulations.

Spatial distribution of land cover

The Manggululiling sub-watershed is dominated by stable forest formations, which serve as the region's primary ecological backbone. Image interpretation from 2020 and 2024 confirms that primary dryland forest consistently remains the most extensive land cover class, occupying 915.65 ha or 47.97% of the total area. This high percentage indicates that the upstream conservation function remains intact and free from significant deforestation pressures. This condition aligns with Indonesian Law No. 41 of 1999, which mandates maintaining a minimum forest area of 30% within a watershed to optimize environmental, social, and economic benefits. Furthermore, the zero reduction in primary forest area observed over the four-year period demonstrates the effectiveness of natural protection mechanisms in safeguarding the main catchment zone. The changes in land cover area between 2020 and 2024 are presented in Table 7.

Beyond primary forests, the watershed exhibits positive vegetation dynamics reflecting natural succession processes. The sub-watershed supports substantial vegetative cover, comprising Shrubs covering 455.11 ha (23.84%) and secondary dryland forest covering 168.78 ha (8.84%). From a silvicultural perspective, the fact that one-third of Neotropical forests are currently secondary forests demonstrates that abandoned agricultural lands or grasslands (open areas) can naturally regenerate through secondary succession. This process gradually establishes young forest stands with increasingly mature ecosystem structures and functions (Poorter et al., 2021). Consequently, the combined extent of primary and secondary forests reaches approximately 56.8%, a figure that far exceeds the ecological adequacy standards for a healthy watershed.

Land use activities, specifically mixed dryland agriculture and paddy fields, collectively account for less than 8% of the total landscape. Although there is a discernible shift in local cropping patterns – characterized by a decrease in paddy fields and a slight expansion of mixed gardens – these

Table 5. Confusion matrix of land cover classification in 2020

Land cover		2020 Google Earth imagery data								Total	User's accuracy
		Primary forest	Secondary forest	Open ground	Settlement	Mixed dryland farming	Savanna/ grassland	Rice fields	Bushes		
20240 land cover classifycation data	Primary forest	84								84	100
	Secondary forest		14							14	100
	Open ground			2		1				3	66.67
	Settlement				1					1	100
	Mixed dryland farming					1				1	100
	Savanna/ Grassland						26			26	100
	Rice fields							5	2	7	71.43
	Bushes			1					47	48	97.92
	Total	84	14	3	1	2	26	5	49	184	
Producer's accuracy		100	100	66.67	100	50	100	100	95.92		180

Table 6. Confusion matrix of land cover classification in 2024

Land cover		2025 land cover observation								Total	User's accuracy
		Primary forest	Secondary forest	Open ground	Settlement	Mixed dryland farming	Savanna/ grassland	Rice fields	Bushes		
2024 Land Cover Classification Data	Primary forest	84								84	100
	Secondary forest		15							15	100.00
	Open ground			2		1				3	66.6667
	Settlement				1					1	100
	Mixed dryland farming					3				3	100
	Savanna/ Grassland						26			26	100.00
	Rice fields							5		5	100
	Bushes		1	1					45	47	95.7447
	Total	84	16	3	1	4	26	5	45	184	
Producer's Accuracy		100	93.75	66.67	100	75	100	100	100		181

Table 7. Changes in land cover area 2020 and 2024

Land cover	2020 (Ha)	Percentage (%)	2024 (Ha)	Percentage (%)
Primary forest	915.65	47.97	915.65	47.97
Secondary forest	163.66	8.57	168.78	8.84
Settlement	7.16	0.38	7.16	0.38
Mixed dryland farming	54.85	2.87	78.09	4.09
Savanna/grassland	210.15	11.01	210.15	11.01
Rice fields	82.89	4.34	58.21	3.05
Bushes	455.05	23.84	455.11	23.84
Open ground	19.47	1.02	15.74	0.82
Total	1908.88	100	1908.88	100

Note: Image interpretation 2020 and 2024.

activities do not encroach upon forest boundaries. Notably, the extent of open land declined from 19.47 ha to 15.74 ha (0.82%) in 2024. This local reduction aligns with the broader conclusion that the declining trend in primary land clearing for mining and oil palm plantations across Indonesia limits the creation of new open lands. Consequently, this indirectly minimizes the risk of surface erosion on sloping terrain and subsequent sedimentation into the nearest river network (Parker et al., 2024). Comparison of land cover maps are presented in Figure 6.

Land cover change analysis

The analysis of land cover changes between 2020 and 2024 demonstrates that the Manggu-liling sub-watershed possesses a high degree of ecological resistance against deforestation pressures. This stability is primarily evidenced by the persistence of primary dryland forest, which maintained a constant area of 915.65 ha (100%) throughout the observation period. The absence of forest conversion within the upstream core conservation zone characterized by steep slopes, high rainfall, and dense vegetation indicates that this area remains intact (Urfan and Ningrum, 2022). From a forestry perspective, the preservation of this primary vegetation is critical, as it functions as the ecosystem responsible for regulating the watershed's base flow and preventing soil erosion. The detailed results of the land cover change analysis are presented in Table 8.

Positive dynamics in forest stand development are further evident through the process of natural succession. The data indicates an increase

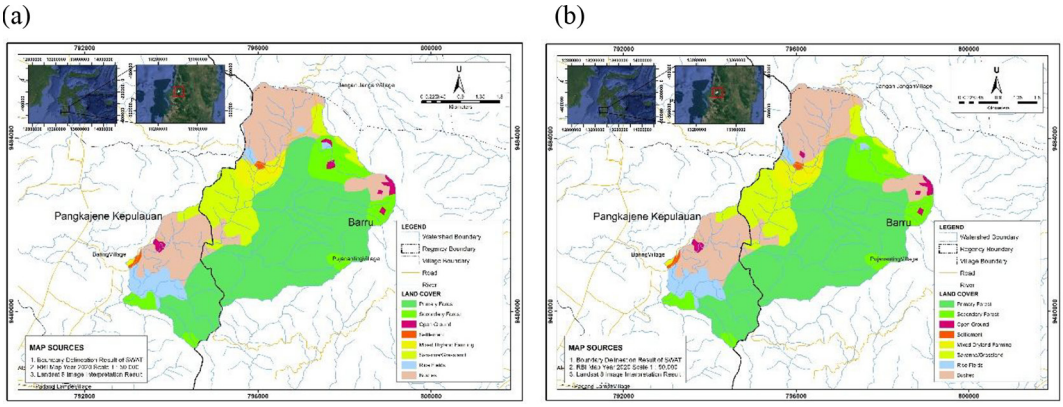

Figure 6. Comparison of land cover maps in the Mangguliling sub-watershed (a) 2020 and (b) 2024

in the extent of secondary dryland forest by 5.11 ha (rising from 163.66 ha to 168.78 ha). The recovery of natural vegetation on degraded lands demonstrates that shrublands and open areas have naturally regenerated into young forest stands dominated by pioneer species (Blackham et al., 2014). Although the Shrub class remained relatively stable, its extensive presence continues to function as a buffer zone separating the area from the protected forest boundary.

Significant land use shifts were identified exclusively within community cultivation zones, rather than in forest areas. There was a substantial reduction in paddy field area by 24.68 ha (declining from 82.89 ha in 2020 to 58.21 ha in 2024), which corresponds with an increase in mixed dryland agriculture by 23.24 ha. This correlation strongly suggests a conversion of wetland agriculture into simple agroforestry systems, driven by abundant water availability and the economic need of farmers to diversify income through a combination of plantation and horticultural crops (Khatun and Palit, 2024). Furthermore, the data indicates a process of ecosystem recovery, where 5.11 ha of open land has naturally transformed into secondary dryland forest. The transition from open land to forest vegetation cover provides significant hydrological benefits by increasing soil infiltration capacity, thereby reducing surface runoff and stabilizing watershed flow (Saputra et al., 2023).

Hydrological response

Water balance components

An evaluation of the water balance components was conducted to analyze the hydrological response of the Mangguliling sub-watershed from 2020 to 2024. This analysis utilized a constant precipitation input to isolate the specific impact of land cover changes on the water cycle. A

Table 8. Land cover change matrix

Land cover 2020	Land cover 2024								
	Primary forest	Secondary forest	Open ground	Settlement	Mixed dryland farming	Savanna/ Grassland	Rice fields	Bushes	Total
Primary forest	915.65								915.65
Secondary forest		163.66							163.66
Open ground		5.11	14.36						19.47
Settlement				7.16					7.16
Mixed dryland farming					54.85				54.85
Savanna/ Grassland						210.15			210.15
Rice fields					23.24		57.35	2.30	82.89
Bushes			1.38				0.86	452.81	455.05
Total	915.65	168.78	15.74	7.16	78.09	210.15	58.21	455.11	1908.88

Note: Image interpretation 2020 and 2024.

summary of the simulation results is presented in Table 9 and Figure 7.

Based on the simulation results, the annual precipitation input was recorded at 2,437.20 mm for both periods. These results indicate that the watershed has maintained a high level of hydrological stability. Land cover changes occurring over the past four years have not had a significant negative impact on the water balance. This ecosystem stability is evident in the Evapotranspiration (ET) values for both 2020 and 2024. The ET value remained constant at 1,195.10 mm, equivalent to 49% of the total precipitation. This consistency suggests that vegetation biomass within the watershed is functioning optimally to return moisture to the atmosphere through high evapotranspiration rates, while simultaneously maintaining a stable microclimate balance (Nath et al., 2021).

Watershed health is also reflected in its flow characteristics. The average curve number (CN) showed negligible change, shifting only slightly from 60.13 in 2020 to 60.14 in 2024. This stability indicates that the soil infiltration capacity remains intact. The volume of surface runoff decreased slightly from 199.98 mm to 199.42 mm, while lateral flow increased from 854.25 mm to 854.91 mm. The dominance of lateral flow, which is significantly higher than surface runoff in the forest, indicates that the forest soil structure effectively absorbs rainwater and channels it as subsurface flow (Saputra et al., 2023). This mechanism is crucial for reducing the risk of flash floods and surface erosion.

Spatial distribution of water yield

The spatial distribution of the annual water yield for the 2020 and 2024 simulation periods is visualized in Figure 8. The maps reveal a distinct spatial heterogeneity across the Manggululiling sub-watershed, driven primarily by the interaction between topographic gradients and land cover characteristics.

The upstream areas (sub-basins 2, 4, and 6), characterized by high elevation and dense forest cover, consistently exhibit the highest water yield values. In the 2024 simulation, values in these regions range from 1,053.99 mm to 1,149.13 mm, while in 2020, they reached up to 1,227.83 mm. This high water yield is largely attributed to the orographic effect, where mountainous regions generate higher extreme rainfall intensities compared to lowlands or coastal areas (Marra et al., 2022). Furthermore, the downstream areas (Subbasins 7 and 9) show relatively lower water yield values. For the 2024 period, these values range from 767.49 mm to 795.55 mm, decreasing from the 2020 range of 842.52 mm to 911.53 mm. The canopy and litter layer of tropical forests in the upstream zone act as a natural sponge that intercepts rainfall, generating significant lateral flow through soil horizons to maintain the hydrological stability of the watershed (Bruijnzeel, 2004).

Evaluation of flow regime and watershed health

River discharge fluctuations

An analysis of river discharge fluctuations was conducted to understand the hydrological response of the Manggululiling sub-watershed to rainfall dynamics and land cover changes between 2020 and 2024. The average monthly discharge depicting these fluctuation patterns is presented in Figure 9. Visually, the discharge fluctuation patterns in 2020 and 2024 reflect the seasonal rainfall distribution (monsoonal type). River discharge experiences a significant increase during the rainy

Table 9. Comparison of water balance components in the Manggululiling sub-watershed

Water balance component	2020 Value (mm)	2024 Value (mm)	Change (mm)
Precipitation	2,437.20	2,437.20	0
Evapotranspiration (ET)	1,195.10	1,195.10	0
Surface runoff	199.98	199.42	-0.56
Lateral flow	854.25	854.91	+0.66
Return flow (base flow)	133.69	133.50	-0.19
Recharge to deep aquifer	9.09	9.09	0
Average curve number (CN)	60.13	6.14	+0.01

Note: Water balance simulation result (SWAT).

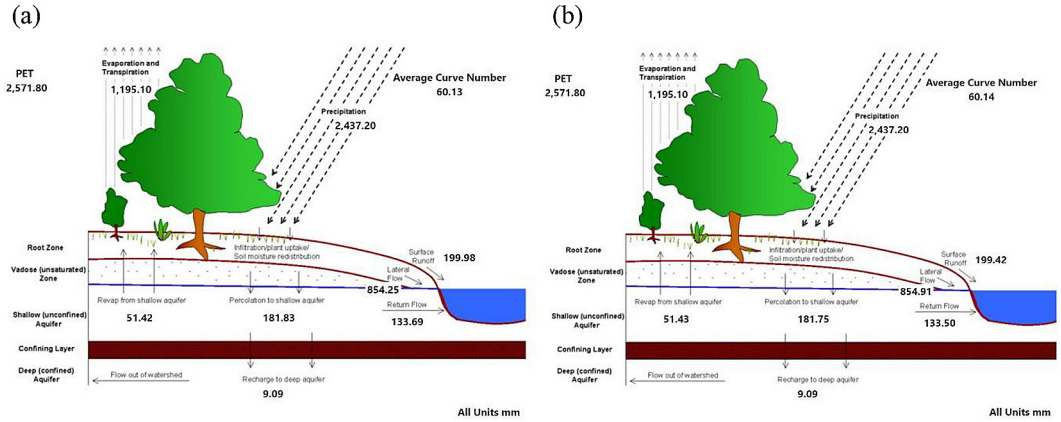

Figure 7. Water balance simulation result (SWAT) (a) 2020 and (b) 2024

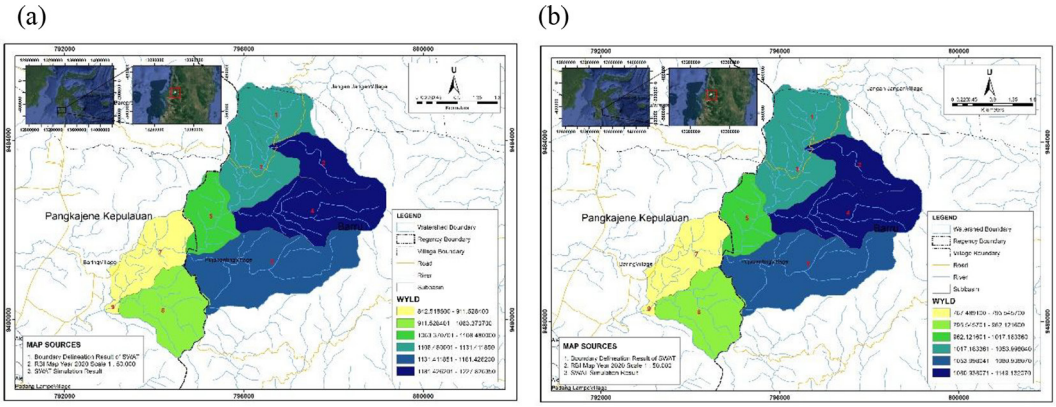

Figure 8. Spatial distribution of annual water yield (a) 2020 and (b) 2024

season (December–February) and undergoes a gradual recession upon entering the dry season.

Based on the simulation results summarized in Table 10, the maximum discharge in 2024 was recorded at 254.31 m³/s in December. This value represents an increase of 29.46 m³/s compared to the 2020 peak discharge of 224.85 m³/s in the same month. This increased fluctuation during the rainy season directly correlates with the extreme rainfall intensity that occurred in late 2024. Despite land cover changes, the stability of the peak flow response indicates that small-scale land conversion in the watershed has not caused drastic changes in flood patterns without being triggered by rainfall anomalies (Saraswati et al., 2025).

During the peak of the dry season in 2024, river discharge dropped sharply, reaching 0.86 m³/s in August. This condition contrasts significantly with the fluctuations in 2020, where the minimum discharge was maintained at a level of 7.87 m³/s in September. This decrease of 7.01 m³/s indicates hydrological stress resulting from the prolonged drought in 2024. However, the persistence of positive baseflow demonstrates that the groundwater storage capacity of the Manggululing watershed remains functional in maintaining streamflow sustainability. In aggregate, the mean annual discharge showed a decline from 70.83 m³/s in 2020 to 65.48 m³/s in 2024. This average decrease of 5.35 m³/s confirms that despite temporary discharge surges during the rainy season, the dominance of a prolonged dry period in 2024 resulted in lower total annual water availability compared to 2020. The wide gap between maximum and minimum discharge in 2024 is what subsequently triggered the significant increase in the RRC value compared to the previous period (Izzatuddinillah and Barus, 2023).

River regime coefficient

The river regime coefficient (RRC) was calculated to evaluate the natural regulatory capacity of the Manggululing sub-watershed in storing and releasing water. RRC is defined as the ratio between the maximum discharge ($Q_{\{max\}}$)

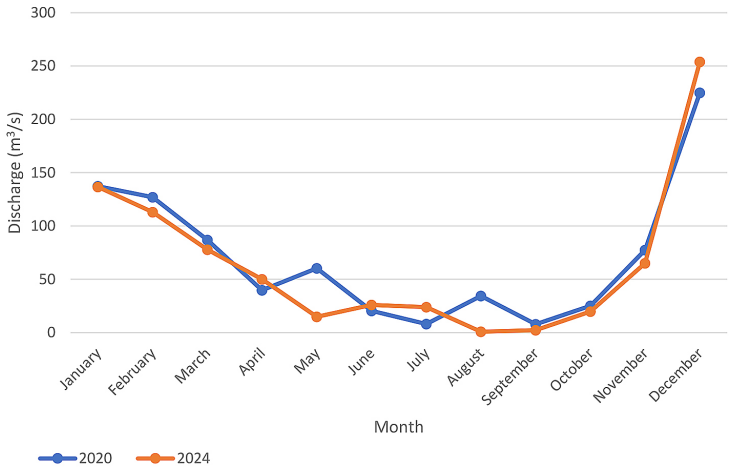

Figure 9. Comparison of monthly discharge in Manggululiling Sub-watershed (2020 and 2024)

Table 10. Summary of SWAT simulation flow parameters 2020 and 2024

Flow parameter	Maximum discharge (m^3/s)	Minimum discharge (m^3/s)	Average discharge
2020 value (m^3/s)	224.85	7.87	70.83
2024 value (m^3/s)	254.31	0.86	65.48

Note: SWAT simulation result.

during the rainy season and the minimum discharge ($Q_{\{min\}}$) during the dry season. The comparison of RRC values derived from the SWAT simulation results for 2020 and 2024 is presented in Table 11.

Based on the calculations in Table 8, the RRC value for the 2024 period was recorded at 295.71. Referring to the standard classification established by the Ministry of Forestry, this value falls into the high (poor) category. This condition stands in sharp contrast to the 2020 period, where the RRC value was only 28.57, classified as low (good). The significant surge in the RRC value in 2024 indicates a drastic decline in watershed flow stability compared to 2020. This extreme increase was primarily driven by the drastic drop in minimum discharge ($Q_{\{min\}}$) to 0.86 m^3/s due to prolonged dry season stress, and further exacerbated by the increase in maximum discharge ($Q_{\{max\}}$) at the end of the year to 254.31 m^3/s. The widening gap between peak and base discharge suggests that during the 2024 simulation period, the watershed experienced high hydrological stress. The highly fluctuating RRC value indicates a significant shift in the watershed's hydrological response status regarding rainfall sensitivity, although land cover changes also contributed (Hidayat, 2024).

Watershed health assessment

Based on the discharge characteristics and flow regime analysis presented previously, a comprehensive watershed health assessment was conducted. This evaluation integrates the runoff coefficient (C) as a proxy for land performance and the *RRC* to represent river stability, in accordance with the standards of the Regulation of the Minister of Forestry No. P.61/ Menhut-II/2014. A summary of the watershed health status comparison between 2020 and 2024 is presented in Table 12.

The evaluation results indicate a significant divergence in the hydrological response of the Manggululiling sub-watershed throughout the observation period.

1. Effectiveness of land hydrological function (C)

The C value, which remained stable at 0.06 (categorized as very low) throughout the observation period, indicates that the hydrological function of land cover in the Manggululiling Sub-watershed is well-maintained. This suggests a high soil infiltration capacity, where forest vegetation and litter effectively regulate water flow rates. This finding is consistent with the theory proposed by (Asdak, 2010), which states that dense forest vegetation with well-developed root structures can enhance soil

Table 11. River regime coefficient Manggululing Sub-watershed

Simulation year	$Q_{\{max\}}$ (m³/s)	$Q_{\{min\}}$ (m³/s)	RRC value	Classes
2020	224.85	7.87	28.57	Low
2024	254.31	0.86	295.71	High

Note: SWAT simulation result based on the criteria of the Ministry of Forestry Regulation No. P.61/2014.

Table 12. Comparison of the hydrological health status of the Manggululing Sub-watershed

Indicator	Year		Description
	2020	2024	
Flow regim coefficient (FRV)	28.57	295.71	Degraded
Runoff coefficient (C)	0.06	0.06	Stable

Note: SWAT simulation result based on the criteria of the Ministry of Forestry Regulation No. P.61/2014.

porosity, thereby increasing the potential for rainfall to infiltrate as groundwater rather than becoming surface runoff. With a *C* value of 0.06, this watershed is capable of absorbing up to 94% of rainfall, significantly minimizing the risk of soil erosion.

2. Discharge fluctuations driven by rainfall variability (*RRC*)

The *RRC* value experienced an extreme surge from 28.57 (Good) in 2020 to 295.71 (Poor) in 2024. This increase in the *FRC* value indicates a wide gap between the maximum discharge ($Q_{\{max\}}$) during the rainy season and the minimum discharge ($Q_{\{min\}}$) during the dry season in 2024. Given that the land cover conditions did not undergo degradation (as shown by the stable *C* value), this instability was strongly driven by climate variability factors, specifically the rainfall distribution pattern. This phenomenon supports the study by (Bruijnzeel, 2004) regarding the "sponge effect," which emphasizes that the ability of forests to regulate water systems has a saturation limit. When climatic anomalies occur, such as extreme rainfall or prolonged drought (as seen in 2024), meteorological factors become more dominant in controlling river discharge compared to land cover factors.

This finding is also consistent with (Sunardi, 2016), who stated that the very high *RRC* values in the Babak watershed – despite having relatively good land cover – are caused by the characteristics of tropical rainfall, specifically high intensity and short duration. Such rainfall exceeds the soil infiltration capacity, causing the river system to provide an immediate peak discharge response.

3. Management implications

The combination of a low *C* value and a high *RRC* confirms that the primary issue in the Manggululing sub-watershed is not forest degradation, but rather water distribution management. Consequently, conservation strategies alone will not be sufficiently effective in reducing the *RRC*. The construction of retention basins as rainwater harvesting structures is required to capture the rainy season's water surplus and distribute it optimally during low-flow periods in the dry season (Ifrayaski, 2019).

CONCLUCIONS

Analysis shows that the Manggululing sub-watershed has a high level of ecological resilience against deforestation pressure. This is evidenced by the area of Primary Dryland Forest, which remained stable at 915.65 ha (47.97%) during the 2020–2024 period. The occurring vegetation change dynamics are positive through natural succession processes, marked by an increase in secondary dryland forest area of 5.11 ha due to the recovery of open land into young forest stands. Other land-use changes only occurred in community cultivation zones, namely the conversion of paddy fields into mixed dryland agriculture covering 23.24 ha.

SWAT model simulation results indicate that the Manggululing sub-watershed is in a stable hydrological condition. Despite small-scale land-use changes, soil infiltration capacity is maintained with relatively constant CN values. The forest's function as a water reservoir operates

optimally, as reflected by the dominance of lateral flow compared to surface runoff. Although there was an increase in maximum discharge in 2024 due to extreme rainfall anomalies, baseflow availability remained stable even during the peak of the dry season, indicating that the groundwater storage function in this region is still functioning effectively.

Acknowledgments

The authors would like to thank Hasanuddin Univresity for the support in providing research facilities and administrative assistance. We extend our gratitude to the Geospatial Information Agency of Indonesia (BIG) for the accessibility of the DEMNAS and RePPProT (Regional Physical Planning Programme for Transmigration) datasets, as well as to NASA for the meteorological data used in this study. The authors also appreciate the constructive comments from the anonymous reviewers which helped improve the quality of this manuscript.

REFERENCES

1. Amelia l. Karouw, Daud M. Liando, Waleleng, G. (2016). Implementation of the Tondano Watershed management policy in North Sulawesi Province. *Journal of Chemical Information and Modeling*, *53*(9), 1689–1699.
2. Asdak, C. (2010). Hydrology and Watershed Management. *Edisi Revisi Kelima, Yogyakarta, Gadjah Mada University Press Yogyakarta*.
3. Bashari, M., Moradi, R. H., Kheirkhah, M. M., Jafari-Khaledi, M. (2013). Temporal variations of runoff and sediment in different soil clay contents using simulated conditions. *Soil and Water Research*, *8*(3), 124–132. https://swr.agriculturejournals.cz/artkey/swr-201303-0004.php
4. Blackham, G. V, Webb, E. L., Corlett, R. T. (2014). Natural regeneration in a degraded tropical peatland, Central Kalimantan, Indonesia: Implications for forest restoration. *Forest Ecology and Management*, *324*, 8–15. https://doi.org/https://doi.org/10.1016/j.foreco.2014.03.041
5. Bruijnzeel, L. A. (2004). Hydrological functions of tropical forests: not seeing the soil for the trees? *Agriculture, Ecosystems & Environment*, *104*(1), 185–228. https://doi.org/https://doi.org/10.1016/j.agee.2004.01.015
6. Hidayat, F., Soma, A. S., Achmad, M., Ramadhan, M. D. R., Abdullah, N. O. (2025). Projections of land cover change and its implications for water yield in the Maros watershed. *Ecological Engineering and Environmental Technology*, *26*(8), 144–159. https://doi.org/10.12912/27197050/207327
7. Hidayat, Y. (2023). Study of river regime coefficients and baseflow index as indicators of watershed performance. *Syntax Literate: Jurnal Ilmiah Indonesia*, *8*(11), 12–25. https://doi.org/https://doi.org/10.36418/syntax-literate.v8i11.15270
8. Hidayat, Y. (2024). Study of river regime coefficients and baseflow indices as indicators of watershed performance. *Syntax Literate; Jurnal Ilmiah Indonesia*. https://doi.org/DOI:10.36418/syntax-literate.v8i11.15270
9. Ifrayaski. (2019). *Optimization of the Pantang Forest Small Dam Operation to Meet Irrigation Water Requirements in the Cubo Trienggadeng Irrigation Area, Pidie Jaya Regency*. *2*(4), 344–351. https://doi.org/https://doi.org/10.24815/jarsp.v2i2.14951
10. Izzatuddinillah, I., Barus, B. (2023). *Analysis of Land Use and Spatial Patterns Based on River Regime Coefficients (RRC) in the Air Bengkulu Watershed*. *25*(2), 56–63. https://doi.org/DOI: http://dx.doi.org/10.29244/jitl.25.2.56-63
11. Khatun, N., Palit, D. (2024). *Wetland-based agroforestry: Carbon management toward sustainability* (M. K. Jhariya, R. S. Meena, A. Banerjee, S. Kumar, A. B. T.-A. for C. and E. M. Raj (eds.); 173–190. Academic Press. https://doi.org/https://doi.org/10.1016/B978-0-323-95393-1.00013-0
12. Latue, P. C., Septory, J. S. I., Rakuasa, H. (2023). Land cover change of Ambon City in 2015, 2019, and 2023. *JPG (Jurnal Pendidikan Geografi)*, *10*(1), 177–186. https://doi.org/10.20527/jpg.v10i1.15472
13. Marra, F., Armon, M., Morin, E. (2022). *Coastal and orographic effects on extreme precipitation revealed by weather radar observations*. 1439–1458. https://doi.org/https://doi.org/10.5194/hess-26-1439-2022
14. Ministry of Forestry. (2014). *Regulation of the Minister of Forestry of the Republic of Indonesia Number P.61/Menhut-II/2014 concerning Monitoring and Evaluation of Watershed Management.* Jakarta: Ministry of Forestry.
15. Miralles-Wilhelm, F., Matthews, J. H., Karres, N., Abell, R., Dalton, J., Kang, S.-T., Liu, J., Maendly, R., Matthews, N., McDonald, R., Muñoz-Castillo, R., Ochoa-Tocachi, B. F., Pradhan, N., Rodriguez, D., Vigerstøl, K., van Wesenbeeck, B. (2023). Emerging themes and future directions in watershed resilience research. *Water Security*, *18*, 100132. https://doi.org/https://doi.org/10.1016/j.wasec.2022.100132
16. Nath, A. J., Kumar, R., Devi, N. B., Rocky, P., Giri, K., Sahoo, U. K., Bajpai, R. K., Sahu, N., & Pandey, R. (2021). Agroforestry land suitability analysis in the Eastern Indian Himalayan region. *Environmental Challenges*, *4*, 100199. https://doi.org/https://doi.org/10.1016/j.envc.2021.100199

17. Nursaputra, M., Syahrul R, A. M., Rijal, S., Fa'iq, M. (2024). Spatial-based hydrological modeling for the identification and analysis of flood-prone areas in the Lamasi Watershed. *Jurnal Sains Informasi Geografi*, *7*(2), 83. https://doi.org/10.31314/jsig.v7i2.3365
18. Parker, D., Tosiani, A., Yazid, M., Sari, I. L., Kartika, T., Firmansyah, R., Said, Z., Wijaya, A., Potapov, P., Tyukavina, A., Stehman, S. V, Zalles, V., Pickens, A., Pickering, J., Turubanova, S., Hansen, M. C. (2024). Land in limbo: Nearly one third of Indonesia's cleared old-growth forests left idle. *Proceedings of the National Academy of Sciences*, *121*(28), e2318029121. https://doi.org/10.1073/pnas.2318029121
19. Pindi, S., Jayakumar, K. V. (2023). Modelling runoff and sedimentation yield using soil and water assessment tool for Wyra River Basin. *Ecological Engineering and Environmental Technology*, *24*(5), 84–93. https://doi.org/10.12912/27197050/165776
20. Poorter, L., Rozendaal, D. M. A., Bongers, F., Almeida, de J. S., Álvarez, F. S., Andrade, J. L., Arreola Villa, L. F., Becknell, J. M., Bhaskar, R., Boukili, V., Brancalion, P. H. S., César, R. G., Chave, J., Chazdon, R. L., Dalla Colletta, G., Craven, D., de Jong, B. H. J., Denslow, J. S., Dent, D. H., … Westoby, M. (2021). Functional recovery of secondary tropical forests. *Proceedings of the National Academy of Sciences of the United States of America*, *118*(49). https://doi.org/10.1073/pnas.2003405118
21. Saputra, N. E., Wibowo, C., Tarigan, S. D., Lisnawati, Y. (2023). A study of land cover change effects on hydrological characteristics in the Gunung Dahu Research Forest. *Jurnal Penelitian Hutan Tanaman*, *20*(1 SE-Articles). https://doi.org/10.59465/jpht.v20i1.312
22. Saraswati, G. S., Asdak, C., Joy, B. (2025). Characteristics of the Air Bengkulu Watershed and Its land use changes in relation to flood events. *Jurnal Ilmu Lingkungan; 23(4) July 2025*. https://doi.org/10.14710/jil.23.4.915-922
23. Sari, A. A., Jamilah. (2023). Study of soil physical properties at several slope inclination classes in smallholder rubber (*Hevea Brasiliensis*) plantations, Sei Bingai Subdistrict, Langkat Regency. *Jurnal Online Agroekoteknologi*, *11*(2337), 1–9. https://doi.org/10.32734/joa.v11i2.9594
24. Sayed, K., Nazimuddin, R., Syakir, M. I., Yusuff, S., Johar, R., Yaseen, Z. M. (2025). Shifting paradigm in water resources management: Public willingness to participate in watershed management of Batu Kurau, Perak, Malaysia. *World Development Perspectives*, *39*, 100694. https://doi.org/https://doi.org/10.1016/j.wdp.2025.100694
25. Soma, A. S., Wahyuni, Musdalifah. (2021). Prediction of erosion and sedimentation rates using SWAT (soil and water assessment tool) method in Malino Sub Watershed Jeneberang Watershed. *IOP Conference Series: Earth and Environmental Science*, *886*(1). https://doi.org/10.1088/1755-1315/886/1/012103
26. Sunardi. (2016). *Analysis of Runoff Coefficients and River Regime Coefficients as Parameters for Assessing Watershed Criticality (A Case Study of the Babak Watershed)*.
27. Susanto, R. D. W. I. (2003). *Identification Of Three Dominant Rainfall Regions Within Indonesia And Their Relationship To Sea Surface*. *1452*, 1435–1452. https://doi.org/10.1002/joc.950
28. Tilahun, A. (2015). Accuracy assessment of land use land cover classification using Google Earth. *American Journal of Environmental Protection*, *4*, 193. https://doi.org/10.11648/j.ajep.20150404.14
29. Urfan, F., Ningrum, A. S. (2022). *Conservation Zone Delimitation Based on Physical Properties in Langsa Watershed, Aceh Province*. *7*(2), 180–193. https://doi.org/https://doi.org/10.19184/geosi.v7i2.31624
30. Zheng, W., Zhang, H., Jiang, Y., Zhang, X., Tong, Y., Zhang, Q. (2019). *Effect of Slope Gradient on Erosion Evolution Process at Microtopographic Tillage Soil Surfaces*. 481–492. https://doi.org/10.4236/jgis.2019.115029